

SuperDARN observations of the two component model of ionospheric convection

A. Grocott¹, M.-T. Walach¹, S. E. Milan²

¹Lancaster University, Lancaster, LA1 4YB, U.K.

²University of Leicester, Leicester, LE1 7RH, U.K.

Key Points:

- The separation of the dawn and dusk ionospheric convection cell foci is found to vary from 4 h to 22 h of magnetic local time
- When the interplanetary magnetic field (IMF) is southwards and auroral westward electrojet weak, the foci move to the dayside
- When the IMF is strongly northwards and the auroral electrojet modestly active, the foci move towards the nightside

Corresponding author: Adrian Grocott, a.grocott@lancaster.ac.uk

This article has been accepted for publication and undergone full peer review but has not been through the copyediting, typesetting, pagination and proofreading process, which may lead to differences between this version and the [Version of Record](#). Please cite this article as doi: [10.1029/2022JA031101](https://doi.org/10.1029/2022JA031101).

This article is protected by copyright. All rights reserved.

Abstract

We use a 20 year database of Super Dual Auroral Radar Network (SuperDARN) observations to investigate the two component model of ionospheric convection. A convection pattern is included in the database if it is derived from at least 250 radar vectors and has a distribution of electric potential consistent with Dungey-cycle twin vortex flow (a negative potential peak in the dusk cell and a positive potential peak in the dawn cell). We extract the locations of the foci of the convection cells from the SuperDARN convection patterns, and compare their dependencies on the north-south component of the interplanetary magnetic field, IMF B_Z , and the SuperMAG auroral electrojet index, SML . We use these parameters to define intervals of expected dayside or nightside dominated reconnection. Our results show that, under conditions favourable for dominant dayside reconnection, the dawn and dusk foci are shifted toward the dayside and that, under conditions favourable for dominant nightside reconnection, the dawn and dusk foci are shifted toward the nightside.

Plain Language Summary

The Earth's upper atmosphere is coupled to the near-Earth space environment – the magnetosphere – via the planet's magnetic field. This magnetic coupling drives a circulation of plasma – the electrically charged component of the atmosphere, called the ionosphere – from day to night across the poles and back again at lower latitudes. This circulation of plasma is a key component of the energy transport in the magnetosphere-ionosphere system. The circulation is not steady, instead changing in strength whilst expanding and contracting due to the time-dependence of the driving mechanisms. To understand these mechanisms we can model the ionospheric circulation and test the models with observations. In this paper we use a 20 year database of ionospheric radar observations of the plasma flow to test one such model – the expanding-contracting polar cap (ECPC) model – and find evidence to support its predictions of separate dayside and nightside components of the flow.

1 Introduction

The expanding contracting polar cap (ECPC) model of ionospheric convection (Cowley & Lockwood, 1992) dictates that transpolar flow (and hence voltage) should be excited when magnetic reconnection changes the topology of the Earth's magnetic field. Dayside reconnection, between the interplanetary magnetic field (IMF) in the solar wind and the Earth's magnetic field opens previously closed terrestrial field lines, appending newly open flux to the magnetopause, which is then carried into the polar cap by an enhanced plasma flow (e.g. Etemadi et al., 1988; Greenwald et al., 1999). Nightside reconnection, between the open field lines of the northern and southern magnetotail lobes, closes previously open field lines which are carried out of the polar cap and back to the dayside by a similar excitation of plasma flows (e.g. Grocott et al., 2002; Gordeev et al., 2011).

The ECPC model describes the basic form that the ionospheric convection cells should take during intervals of dominant dayside or nightside reconnection as illustrated in, for example, Figure 2 of Lockwood and McWilliams (2021) and as also evident in Figure 1 of this paper (discussed further below). According to the model, when dayside reconnection is dominant the foci of the twin-vortex convection cells are expected to be displaced towards the dayside and when nightside reconnection is dominant the foci of the twin-vortex convection cells are expected to be displaced towards the nightside. The aim of the present study is to determine whether this two-component model of ionospheric convection predicted by the ECPC model is apparent in the SuperDARN ionospheric convection observations.

61 The idea that solar wind - magnetosphere coupling drives magnetospheric and iono-
62 spheric convection is not disputed. It is relatively straightforward to show that the strength
63 of the ionospheric convection (e.g. MacDougall & Jayachandran, 2001) or transpolar volt-
64 age, V_{PC} (e.g. Boyle et al., 1997) is related to the concurrent solar wind and IMF con-
65 ditions. Difficulties arise in isolating the separate contributions from dayside and, in par-
66 ticular, nightside reconnection. Whilst dayside reconnection rates are simple to estimate
67 from upstream solar wind and IMF observations (e.g. Milan et al., 2012), dayside driv-
68 ing tends to precipitate nightside reconnection. Statistical results, such as those of Boyle
69 et al. (1997) and larger-scale models of convection (e.g. Greenwald et al., 1996; Ruohoniemi
70 & Greenwald, 2005; Weimer, 2005; Thomas & Shepherd, 2018) therefore tend to reveal
71 a somewhat steady-state approximation to the response to solar wind driving.

72 Isolating and quantifying the nightside reconnection contribution is a particular chal-
73 lenge, owing in part to a difficulty in measuring the nightside reconnection rate, or es-
74 timating it from in-situ observations. In a study of transpolar voltage data from the Su-
75 per Dual Auroral Radar Network (SuperDARN) Lockwood and McWilliams (2021) used
76 the AL auroral electrojet index as a proxy for the nightside reconnection rate. They used
77 hourly means to show that V_{PC} increases both for increasingly negative IMF B_Z , and
78 increasingly negative AL index, consistent with both dayside and nightside reconnection
79 being responsible for driving convection, as predicted by the ECPC model. A difficulty
80 in interpreting this result arises from the fact that taking hourly averages significantly
81 smoothes structures in the data, especially high values, since V_{PC} is not normally dis-
82 tributed. It is also the case that AL and IMF B_Z are not independent; intervals of strongly
83 negative IMF B_Z correlate with intervals of enhanced AL index. Lockwood and McWilliams
84 (2021) attempt to mitigate this by considering that V_{PC} increases with increasing strength
85 of AL index even for a fixed value of IMF B_Z . However, this does not account for the
86 possibility that factors additional to IMF B_Z strength may directly affect the dayside
87 reconnection rate (e.g. Borovsky et al., 2008).

88 In this paper we use a 20 year archive of SuperDARN radar data to provide direct
89 evidence for the two component model of ionospheric convection. We locate the convec-
90 tion cell foci in the SuperDARN observations and investigate the statistics of their lo-
91 cation, in the context of the transpolar voltage, solar wind and geomagnetic observations.
92 For simplicity, and in order to make direct comparisons with the findings of Lockwood
93 and McWilliams (2021), we use IMF B_Z and the SuperMAG derived AL index (here-
94 after referred to as SML) as proxies for the strength of dayside and nightside reconec-
95 tion. We find that significant voltages may be driven for both dayside and nightside dis-
96 placed convection cell foci. The foci tend to be displaced towards the dayside when IMF
97 B_Z is negative and SML small. They tend to be displaced towards the nightside when
98 IMF B_Z is positive and SML modest. The dawn and dusk cell foci do not appear to re-
99 spond in the same way to differing driving conditions, making the overall behaviour of
100 the convection patterns non-trivial to interpret.

101 2 Data Analysis

102 Large-scale observations of ionospheric convection from 1999-2018 are provided by
103 the Super Dual Auroral Radar Network (SuperDARN). SuperDARN is an international
104 array of HF ionospheric radars located in the polar regions of both hemispheres whose
105 fields-of-view cover much of the polar, auroral and subauroral regions. Each radar mea-
106 sures the line-of-sight (LOS) Doppler velocity of ionospheric plasma irregularities from
107 which the radars scatter (Greenwald et al., 1995; Chisham et al., 2007). The radars scan
108 through typically 16 beams (look directions) making observations at typically 75 loca-
109 tions along each beam at between 180 km and over 3500 km in range. The LOS veloc-
110 ities are derived from best fit autocorrelation functions of the backscattered radar sig-
111 nals. To produce large-scale convection maps, the line-of-sight velocities are median fil-
112 tered at 2-min cadence onto an equal area polar grid of cell size $\sim 110 \times 110$ km. The

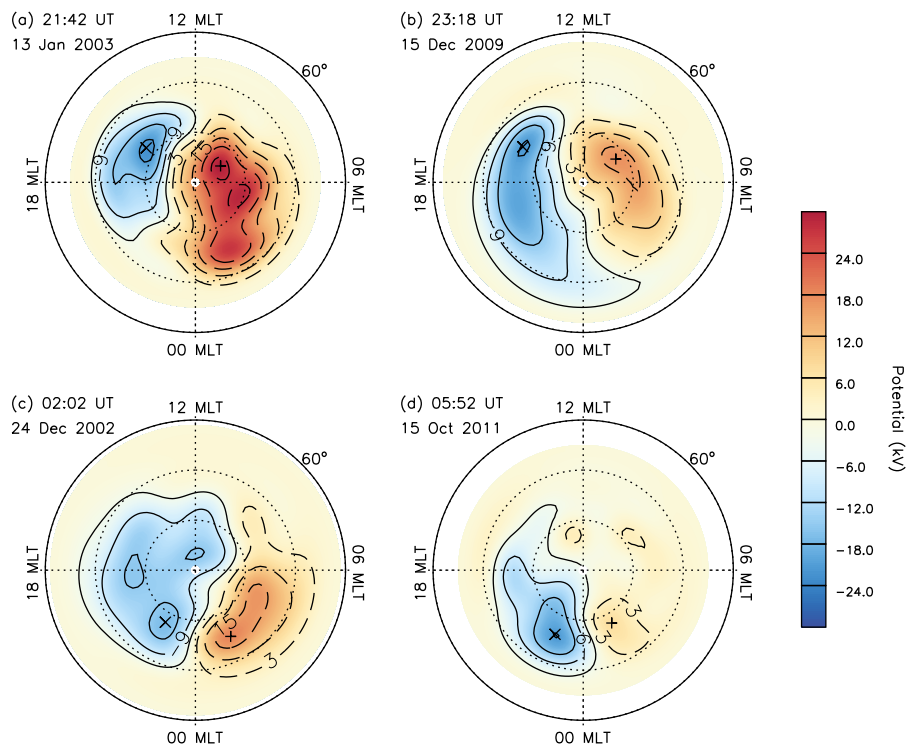


Figure 1. A set of example ionospheric convection maps illustrating the locations of the foci of the dawn and dusk convection cells in terms of the peak values of the positive (orange-red) and negative (blue) electric potential. The maps are presented in geomagnetic longitude - local time coordinates with noon the the top and dawn to the right, from 60 degrees latitude to the pole. In panes (a,b) the foci are located on the dayside, indicative of dominant dayside reconnection. In panels (c,d) the foci are located on the nightside, indicative of dominant nightside reconnection.

latitudinal extent of the convection is determined by fitting a ‘Heppner-Maynard’ boundary to the gridded velocities (see Heppner & Maynard, 1987; Shepherd & Ruohoniemi, 2000). A best-fit spherical harmonic expansion of the ionospheric electric potential is then derived from the radar data (Ruohoniemi & Baker, 1998). Information from a statistical convection model (Thomas & Shepherd, 2018), parameterised by IMF conditions, is used to supplement the radar observations to ensure sufficient coverage of data for the spherical harmonic fit to converge. Full details of the convection mapping software are provided by SuperDARN Data Analysis Working Group et al. (2018) with the processing steps followed in this study being detailed in Walach et al. (2022).

From our convection map archive we extract the magnetic latitude and magnetic local time (MLT) of the peaks of the positive and negative electric potential. We then impose a number of criteria by which we reduce the data set. We first remove any maps for which the total number of gridded radar vectors, n , is less than 250. This criterion removes maps which are more likely to be dominated by the statistical convection model used in the fitting. Similar thresholds have been employed in previous studies (e.g. Imber et al. (2013) used $n > 200$, Lockwood and McWilliams (2021) used $n > 255$, and Fogg et al. (2020) used $n > 400$). A sensitivity test of our results to the choice of n (not shown) suggests no significant difference when using $n > 250$. We then impose the condition that the MLT of the positive potential peak be less than 12 h, and that the MLT of the negative potential peak be greater than 12 h. This is done to maximise the likelihood that the positive and negative potential peaks identified correspond, respectively, to the foci of the dawn and dusk Dungey-cycle twin vortex convection cells.

The resulting data set is then further subdivided by concurrent IMF conditions and geomagnetic activity levels. For this purpose, we use IMF data provided by the Magnetic Fields Experiment (Smith et al., 1998) on board the Advanced Composition Explorer (ACE) spacecraft (Stone et al., 1998) and the SuperMAG derived auroral electrojet index (SML) (Davis & Sugiura, 1966; Newell & Gjerloev, 2011; Gjerloev, 2012). In particular, we define ranges of IMF B_Z and SML index within which we expect either dayside or nightside reconnection to be dominant. For dominant dayside reconnection we suppose that IMF B_Z will be negative, leading to open flux loading of the magnetosphere, whilst SML will be small, indicating no significant development of the nightside westward electrojet. For dominant nightside reconnection we suppose that IMF B_Z will be positive, such that open flux production is switched off (or significantly reduced) whilst SML will be large (and negative), indicative of substorm activity and associated open flux destruction in the magnetotail. The specific range of each parameter used is summarised in Table 1 and discussed in further detail in section 3, below.

Label	IMF B_Z	SML	Description
Dayside	$B_Z < -2$ nT	$SML > -30$ nT	Open flux loading via reconnection at the dayside magnetopause
Nightside	$B_Z > 4$ nT	$-50 > SML > -100$ nT	Open flux unloading via reconnection in the magnetotail

Table 1. Ranges of IMF B_Z and SML index used to filter for intervals of dominant dayside or nightside reconnection.

Example SuperDARN convection patterns from which the dawn and dusk cell foci are extracted are presented in Figure 1. Panels (a,b) are from the subset expected to cor-

151 respond to dominant dayside reconnection. Panels (c,d) are from the subset expected
 152 to correspond to dominant nightside reconnection. It is apparent that in panels (a,b) the
 153 foci are located on the dayside, whereas in panels (c,d) the foci are located on the night-
 154 side. This is consistent with the expectations of the ECPC model as discussed in sec-
 155 tion 1. In the next section we investigate the extent to which this dependence of the cell
 156 foci locations on IMF B_Z and SML holds more generally.

157 3 Results

158 Figure 2 presents an overview of the convection cell foci statistics. All panels are
 159 presented in magnetic latitude, magnetic local time coordinates, with a grid cell size of
 160 1 h of local time and 5° of latitude. Overlaid on each panel for reference is a model kp=2
 161 Feldstein and Starkov (1967) oval. In panel (a) we show the full distribution of the data
 162 set which, after the filtering outlined in section 2, contains over 400,000 convection maps
 163 ($\sim 8\%$ of the total). A wide range of cell foci locations exist, with 97% of dusk foci (and
 164 98% of dawn foci) lying in the latitude range $70^\circ - 85^\circ$, and 97% of dusk foci (95% of
 165 dawn foci) lying in the MLT range 14 - 22 h (2 - 10 h).

166 Figure 2b-c show the subsets of the data after filtering for conditions of IMF B_Z
 167 and SML index expected to yield dominant (b) dayside and (c) nightside reconnection.
 168 In panel (b) we can see that the range of foci latitudes and local times has been reduced
 169 compared to the full data set in panel (a). The foci in (b) tend to be limited to higher
 170 latitudes, indicative of a smaller polar cap. Although the distribution of foci locations
 171 spans the dusk-dawn meridian both to the dayside and nightside, there is a slight ten-
 172 dency towards the dayside with 56% of dawnside foci and 59% of duskside foci being lo-
 173 cated closer to noon than to midnight. In panel (c) we can see that the foci tend to be
 174 at lower latitudes than in panel (b). Although the foci local times still exhibit some spread,
 175 they are more often located on the nightside, with 75% of dawnside foci and 79% of dusk-
 176 side foci located closer to midnight than to noon.

177 Figure 2d-g presents four examples of how the convection cell foci might exhibit
 178 a dependency on the IMF and geomagnetic activity. In each panel, the data set from panel
 179 (a) is now colour-coded to the median value in each grid cell of (d) IMF B_Z , (e) SML
 180 index, (f) IMF B_Y and (g) Sym-H index. To minimise the effect of small statistics un-
 181 duly influencing the results we colour cells containing fewer than 500 values grey. Panel
 182 (d) indicates that, for the dusk cell in particular, strongly negative B_Z favours lower-
 183 latitude, dayside convection cell foci, with positive B_Z favouring nightside foci. Any dawn
 184 cell focus dependency is less apparent. Cells close to dawn generally correspond to weakly
 185 negative B_Z and cells nearer to midnight weakly positive B_Z , but there is also a pop-
 186 ulation of cells closer to noon corresponding to weakly positive B_Z . Panel (e) suggests
 187 that when SML is more strongly negative, the convection cell foci (and hence polar cap
 188 boundary) tends to be at lower latitudes. However, there is no clear tendency for more
 189 nightside located foci at more negative SML values. Panel (f) reveals an IMF B_Y -dependent
 190 rotation of the convection pattern, with positive B_Y producing a clockwise rotation (dusk
 191 foci closer to noon and dawn foci closer to midnight) and negative B_Y producing an an-
 192 ticlockwise rotation (dusk foci closer to midnight and dawn foci closer to noon), but with
 193 no tendency for both foci to be closer to either noon or midnight. Lastly, panel (g) shows
 194 that the foci latitude decreases with increasingly negative Sym-H, with no obvious cor-
 195 relation with the foci local times.

196 The data presented in Figure 2 are suggestive of a dependence of the foci local times
 197 on IMF and geomagnetic activity, but also of the specifics of that dependence being non-
 198 trivial. In Figure 3 we therefore explore this dependence in more detail. Figure 3a-b show,
 199 respectively, the distributions of the dawn and dusk convection cell foci local times (which
 200 we henceforth refer to as CCFLT for brevity). In each case the CCFLT data are plot-
 201 ted versus SML and IMF B_Z , with cells containing fewer than 30 values omitted. The

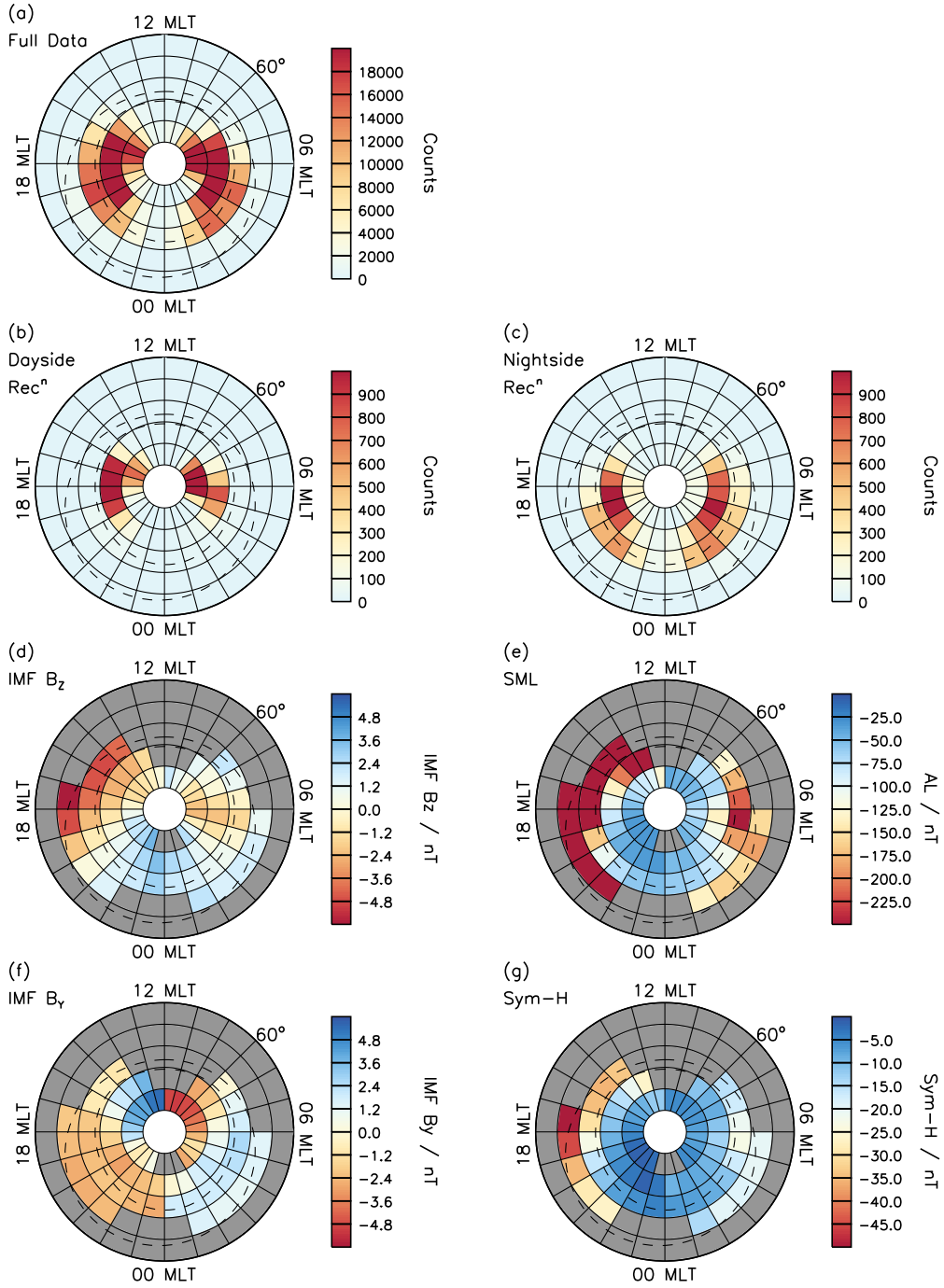


Figure 2. Distributions of the convection cell foci presented in a magnetic latitude, magnetic local time grid, with a model $k_p=2$ Feldstein and Starkov (1967) oval shown for reference. (a) the distribution of all dusk and dawn cell foci included in the data set, (b) and (c) subsets of (a) that have been subject to filtering based on IMF B_z and SML to correspond to expected intervals of dominant reconnection on the dayside and nightside, respectively, (d) - (g) median parameters in each grid cell of panel (a): (d) IMF B_z , (e) SML , (f) IMF B_y , (g) $Sym-H$ (cells containing fewer than 500 values are shaded grey).

202 first thing to note is that there is an interdependence of SML and B_Z , with strongly positive
 203 B_Z only occurring for weak SML and strongly negative SML only occurring for
 204 negative B_Z . This inherently limits the possible dependencies of the CCFLT on the two
 205 parameters. At modest levels of SML there is a clear dependence of the CCFLT on B_Z .
 206 The dawn CCFLT moves from being located close to dawn for negative B_Z into the predawn
 207 sector for positive B_Z . Likewise, the dusk CCFLT moves from being located close to dusk
 208 for negative B_Z to the postdusk sector for positive B_Z . The dawn CCFLT shows very
 209 little dependence on SML . There is some indication that at the weaker end of the SML
 210 range the CCFLT are slightly shifted towards the dayside. This would be consistent with
 211 weak SML being indicative of a lack of nightside reconnection, but negative of about
 212 -100 nT there is little further discernible trend. The dusk CCFLT seem to respond less
 213 to changes in SML . Moving from weak SML to more strongly negative SML at a fixed
 214 weakly positive B_Z the CCFLT actually move towards the dayside. This is counter to
 215 what is expected, if increasingly negative SML was indicative of more dominant night-
 216 side reconnection.

217 In Figure 3c we attempt to combine the information about the dusk and dawn CCFLT
 218 into a single parameter, to quantify the extent to which the foci are closer to the day-
 219 side or nightside. We define a quantity $dMLT$ which is the hour angle, or difference in
 220 hours of local time, between the dusk and dawn cell foci, or $CCFLT_{dusk} - CCFLT_{dawn}$,
 221 such that $dMLT = 12$ h corresponds to convection cell foci that lie along a meridian
 222 line. This might be the dawn-dusk meridian or, if the convection pattern is rotated about
 223 the pole, then one cell's focus would be displaced towards noon to the same extent that
 224 the others cell's focus was displaced towards midnight. Values of $dMLT < 12$ h then
 225 represent a convection pattern where the CCFLT are offset towards the dayside, or at
 226 least, where one cell's focus is displaced towards noon to a greater extent than the other's
 227 is displaced towards midnight. Similarly, $dMLT > 12$ h represents a convection pat-
 228 tern where the CCFLT are offset towards the nightside, or at least, where one cell's fo-
 229 cus is displaced towards midnight to a greater extent than the other's is displaced to-
 230 wards noon.

231 Figure 3c shows that for the majority (67%) of negative IMF B_Z conditions, the
 232 CCFLT separation, $dMLT$, is less than 13 h. When SML is weak (> -30 nT) and B_Z
 233 moderately negative (e.g. < -2 nT), $dMLT$ is less than 12 h (11.5 h median value). This
 234 informed our choice of IMF $B_Z < -2$ nT and $SML > -30$ nT for our dayside recon-
 235 nection filter. As SML becomes increasingly negative, up to ~ -400 nT, so B_Z must
 236 be increasingly negative for $dMLT$ to remain less than 12 h (i.e. red colors on the left
 237 side of the plot). For SML index below ~ -400 nT, however, it appears that $dMLT$
 238 becomes less sensitive to B_Z , with $dMLT$ remaining less than 12 h for increasingly weaker
 239 B_Z . For SML index below ~ -600 nT it appears that $dMLT$ may be less than 12 h for
 240 any value of negative B_Z . When B_Z is positive, $dMLT$ is typically (72% of the time)
 241 greater than 12 h, with the largest values occurring for $B_Z > 4$ nT and $-50 > SML > -100$ nT
 242 (14.8 h median value). This informed our choice of nightside reconnection filter. As SML
 243 becomes increasingly negative below ~ -200 nT, $dMLT$ decreases.

244 In Figure 4 we inspect the behaviour of $dMLT$ in more detail. In (a) we show the
 245 joint probability distribution of V_{PC} and $dMLT$ and in (b) we show the marginal dis-
 246 tributions of the $dMLT$ data subsets. The vertical dashed line in both panels marks $dMLT =$
 247 12 h. V_{PC} here is derived from the SuperDARN convection maps according to $V_{PC} =$
 248 $V_{max} - V_{min}$, i.e. it is the difference between the electric potentials of the dawn and dusk
 249 foci. The distribution of V_{PC} appears to be multimodal, with major peaks at $dMLT \sim$
 250 11 h and $dMLT \sim 13$ h and with a local minimum at 12 h. At the same time, the high-
 251 est V_{PC} values occur for $dMLT$ values close to 12 h. For earlier and later $dMLT$ val-
 252 ues, the peak V_{PC} values decrease. Dayside driving seems to be limited to a small range
 253 of $dMLT$, whereas nightside $dMLT$ values occur over a wider range. In particular, a sec-
 254 ond small population of weaker V_{PC} exists at large $dMLT$ values of $\sim 16 - 18$ h.

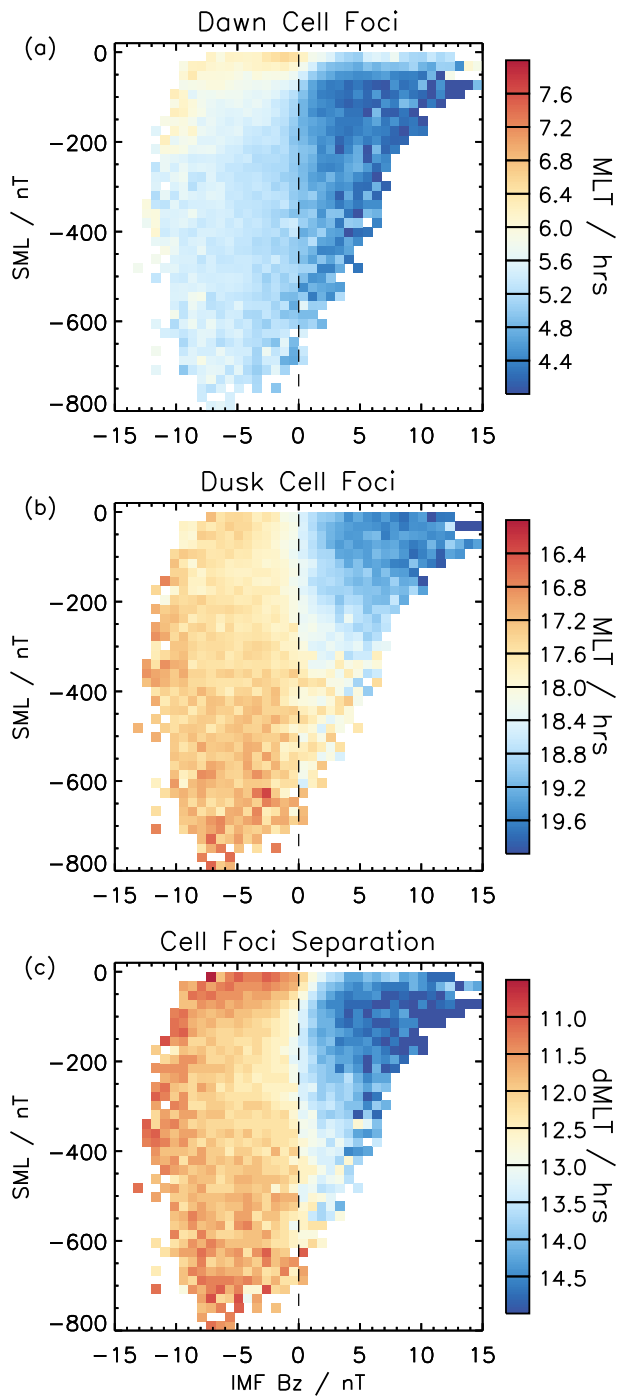


Figure 3. Distributions of the convection cell foci magnetic local times plotted versus SML and IMF B_z for (a) the dawn cell and (b) the dusk cell. (c) hours of separation of the dawn and dusk cells, $dMLT$. Cells containing fewer than 30 values are omitted.

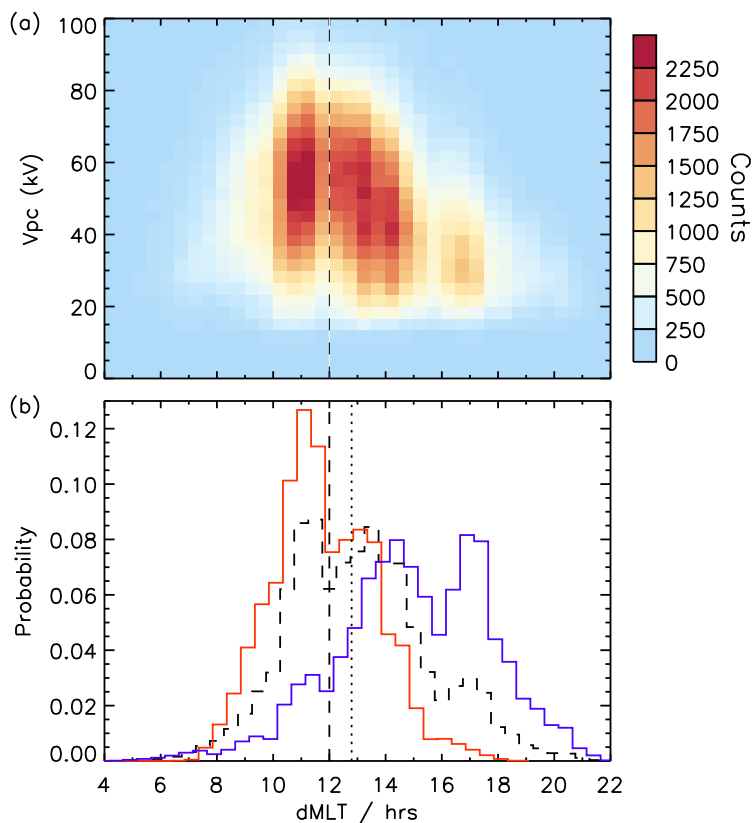


Figure 4. Probability distributions of the dawn-dusk foci separation, $dMLT$. The full data set from Fig.2a is shown as a black dashed line and the filtered data sets from Fig.2b and c are shown by the solid red (dayside reconnection) and blue (nightside reconnection) lines, respectively. The vertical dashed line marks 12 MLT. The vertical dotted line marks the mean $dMLT = 12.8$ h.

255 The marginal distribution of $dMLT$ values for the full data set from Fig.2a is shown
 256 as a dashed black line in Figure 4b. This is consistent with the broad nature of the dis-
 257 tributions of CCFLT. Shown in red is the distribution of the data subset from Fig.2b fil-
 258 tered for dominant dayside reconnection. The distribution is somewhat narrower, and
 259 is shifted to smaller $dMLT$, consistent with the cell foci being closer to the dayside. Shown
 260 in blue is the distribution of the data subset from Fig.2c filtered for dominant nightside
 261 reconnection. This distribution is still quite broad, and does overlap with the dayside
 262 distribution, but is overall shifted to larger $dMLT$, consistent with the cell foci being closer
 263 to the nightside.

264 In Figure 5 we explore whether the overlap between the dayside and nightside re-
 265 connection filtered $dMLT$ values is reflected in the separate dawn and dusk CCFLT,
 266 or whether individually they form discrete populations. Panel (a) presents the the full
 267 data set from Fig. 2a, with the dusk CCFLT plotted against the dawn CCFLT. This shows
 268 that, whilst the dusk cell focus is found with similar prevalence in the afternoon (47%)
 269 and evening (53%) sectors, the dawn cell focus is less often located on the dayside (35%),
 270 being more often predawn (65%). An intrinsic asymmetry is apparent in the foci loca-
 271 tions, in that the most populous quadrant of the distribution is pre-dawn/pre-dusk (33%),

272 consistent with a clockwise rotation of the convection pattern. This compares to only
 273 21% in the post-dawn/post-dusk quadrant that corresponds to an anticlockwise rota-
 274 tion. The post-dawn/pre-dusk quadrant (dayside foci) contains just 14% of the data, whereas
 275 the pre-dawn/post-dusk quadrant (nightside foci) contains 32% of the data.

276 In Figure 5b-c we show similar plots for the (b) dayside and (c) nightside recon-
 277 nection filtered subsets from Fig.2b and c. The nightside subset (panel c) clearly shows
 278 the expected behaviour, with 58% of the data located in the pre-dawn/post-dusk quad-
 279 rant (corresponding to $dMLT > 12$ h) and only 5% in the post-dawn/pre-dusk quad-
 280 rant (corresponding to $dMLT < 12$ h). The behaviour of the dayside subset (panel b)
 281 is less clear cut, with only 30% in the post-dawn/pre-dusk quadrant. A similar propor-
 282 tion of this subset (29%) is in the pre-dawn/pre-dusk quadrant, similar to panel (a). This
 283 is consistent with the absence of any significant dawn CCFLT > 6 h for any combina-
 284 tion of B_Z or SML as noted in reference to Fig. 3. Nevertheless, it is very much appar-
 285 ent that the dayside subset is quite distinct from the nightside subset, with only 15%
 286 in the pre-dawn/post-dusk (nightside) quadrant where most of the nightside subset is
 287 located. A two-sample Kolmogorov-Smirnov test (Press et al., 2007) of the dayside and
 288 nightside subsets supports this assertion, indicating a zero likelihood that the two sub-
 289 sets could be drawn from the same probability distribution.

290 4 Discussion

291 The primary aim of this study was to determine whether the two-component model
 292 of ionospheric convection predicted by the ECPC model is apparent in SuperDARN iono-
 293 spheric convection observations. Using the locations of the peaks in electric potential as
 294 proxies for the convection cell foci, we have presented statistics of the locations of the
 295 foci from which we can draw a number of conclusions. Firstly, as shown in Figure 2a,
 296 the distribution of foci locations is revealed by the SuperDARN data to be quite wide,
 297 despite our pre-selection criteria for the foci having reduced the data to 8% of the total
 298 available. The spread of latitudes of the foci indicate a range of polar cap sizes and
 299 the spread of local times is consistent with convection being driven from both the day-
 300 side and nightside. In order to isolate the convection patterns associated with dominant
 301 dayside and nightside reconnection we have inspected the dependence of the locations
 302 of the convection cell foci on a number of parameters. It is apparent from Figure 2d-e,
 303 however, that no single parameter can explain the observations.

304 Figure 2d suggests that IMF B_Z does exhibit some control, being more positive for
 305 foci locations on the nightside. This is consistent with the idea that the Dungey cycle
 306 can be maintained even during intervals of positive IMF B_Z , but that dayside low-latitude
 307 reconnection will be inactive, or at a low enough rate that nightside reconnection will
 308 be dominant (e.g. Grocott et al., 2002, 2003). When B_Z is negative, and the dayside re-
 309 connection rate is high, we might expect the foci to be located on the dayside. This seems
 310 to be the case for the dusk cell, but appears not to be the case for the dawn cell, for which
 311 moderately negative B_Z correspond to foci being located close to dawn. The lower mag-
 312 nitude of the B_Z averages on the dawn side also suggests that the dawn cell location is
 313 less strongly correlated with B_Z . We consider this apparent dawn - dusk asymmetry fur-
 314 ther, below.

315 Figure 2e shows a dependence of the foci locations on the SML index. In this case,
 316 the dependence appears to more strongly control the latitude of the foci, with SML be-
 317 ing of lower magnitude for higher latitude foci and larger magnitude for lower latitude
 318 foci. There is little evidence that the SML index alone has any influence on the local
 319 time of the foci. This relationship is very similar to the relationship with Sym-H shown
 320 in panel (g). Sym-H is a proxy for the ring current strength (Iyemori, 1990) and as such
 321 is a more global measure of geomagnetic activity that will tend to be high when the po-
 322 lar cap is expanded and both dayside and nightside reconnection are active (e.g. Walach

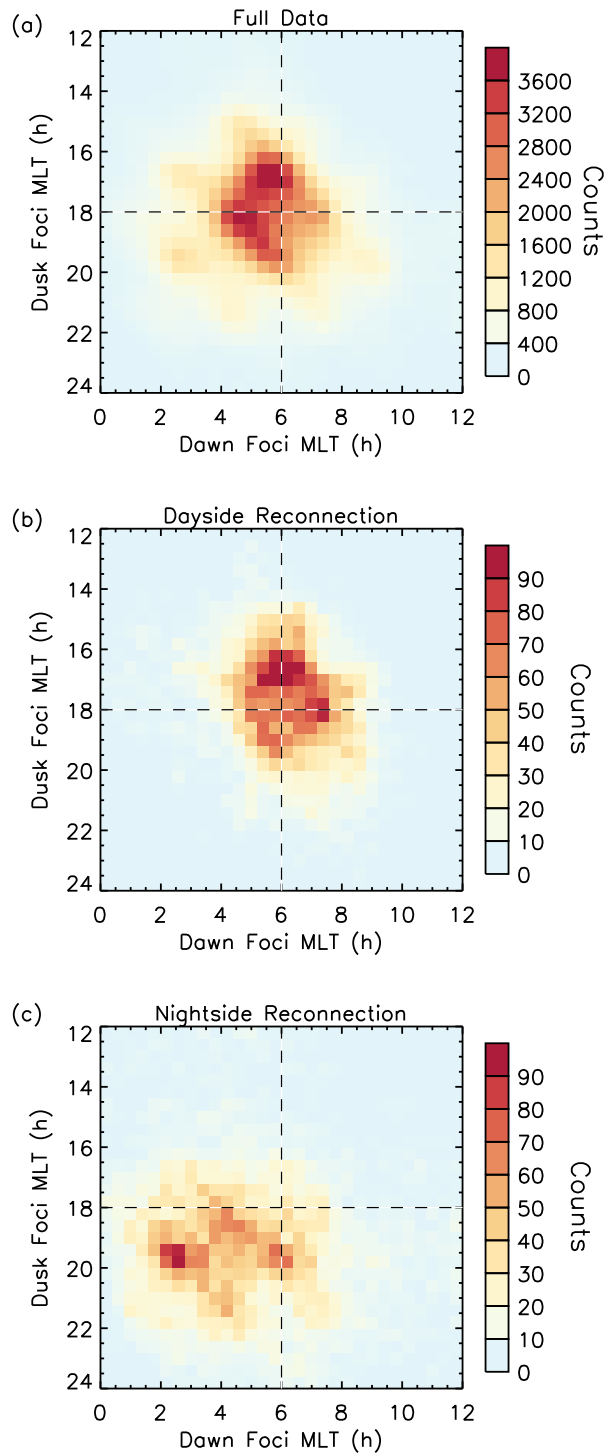


Figure 5. Occurrence distributions of coincident dawn and dusk convection cell foci magnetic local times. (a) the full data set from Fig.2a, (b) the dayside and (c) the nightside reconnection filtered data sets from Fig.2b and c, respectively.

323 & Grocott, 2019), although there is some evidence that nightside reconnection may be
 324 suppressed on shorter timescales when Sym-H is high (e.g. Nakai & Kamide, 2003; Mi-
 325 lan et al., 2008). That the pattern of *SML* index resembles the Sym-H pattern is indica-
 326 tive of an inherent dependence of *SML* on B_Z , certainly on average and, as we discuss
 327 below, even on much shorter timescales, such that increasingly negative *SML* is always
 328 more likely for increasingly negative IMF B_Z . This suggests that although nightside re-
 329 connection is expected to become enhanced with increasingly negative *SML*, it does so
 330 in response to enhanced dayside reconnection. This coupled nature of the nightside and
 331 dayside reconnection serves to complicate efforts to disentangle the contribution of each
 332 to the ionospheric convection pattern.

333 To better understand the interdependency of the *SML* index and IMF B_Z we pre-
 334 sented in Figure 3a-b the distributions of the dawn and dusk convection cell foci local
 335 times (CCFLT), respectively, with respect to *SML* and B_Z . These data revealed a de-
 336 gree of complexity in the relationships and we comment on a few key findings here. First,
 337 the differing behaviour of the dawn and dusk cell foci is readily apparent. The dusk cell
 338 focus is less often on the nightside and, contrary to expectations that enhanced (nega-
 339 tive) *SML* should indicate dominant nightside reconnection, the focus is generally only
 340 on the nightside for weaker *SML* values above ~ -200 nT, and only if B_Z is also posi-
 341 tive. When *SML* is more strongly negative, the dusk focus tends to be on the dayside.
 342 This is therefore more consistent with enhanced dayside reconnection and suggests that
 343 more elevated levels of nightside reconnection are themselves triggered by intervals of
 344 strong dayside reconnection, such that strongly negative *SML* is necessarily accompa-
 345 nied by negative B_Z and similar or even greater levels of dayside reconnection.

346 This tendency for strong *SML* to be often associated with an apparent absence
 347 of dominant nightside reconnection is also apparent in the *dMLT* data in Figure 3c. For
 348 example, if we consider a fixed IMF B_Z value, e.g. $B_Z = 0$, we see that below ~ -200 nT,
 349 as *SML* becomes increasingly negative, *dMLT* tends to decrease. This suggests either
 350 a weakening of nightside reconnection, or a strengthening of dayside reconnection. This
 351 appears contrary to the conclusion of Lockwood and McWilliams (2021) that an increase
 352 in V_{PC} with increasing *AL* magnitude at a fixed IMF B_Z was indicative of dominant night-
 353 side reconnection driving the convection. We suggest that this is a result of the intrin-
 354 sic dependence of *AL* (or *SML*) on B_Z , in that strong *SML* requires as a prerequisite
 355 strong dayside driving as well. This is consistent with the results of Milan et al. (2021)
 356 who studied the magnetospheric flux throughput in the Dungey cycle for a variety of con-
 357 vection states during the year 2010. We further suggest that considering a fixed value
 358 of, e.g., IMF B_Z is insufficient to ensure a fixed level of dayside driving. Otherwise an
 359 increased magnitude of *SML* ought not be associated with a smaller *dMLT*. This is fur-
 360 ther evidenced by considering that below *SML* values of ~ -600 nT it appears that *dMLT* $<$
 361 12 h can occur for any value of negative B_Z . In other words, dayside driving must be high
 362 to produce such a large magnitude *SML* irrespective of the strength of IMF B_Z .

363 The upshot of this analysis is that the determination of suitable limits of IMF B_Z
 364 and *SML* index to be used as filters for intervals of dominant dayside and nightside re-
 365 connection is not straightforward. It seems that in general, the convection cell foci will
 366 be on the dayside for negative B_Z irrespective of *SML*. However, it is true that for mod-
 367 est *SML*, down to ~ -200 nT, the average *dMLT* increases, presumably as a result
 368 of the contribution of nightside reconnection driven flows. The simplest way to ensure
 369 a predominance of dayside reconnection driven flows is thus to place a strict limit on the
 370 value of *SML*, and as such we have used *SML* > -5 nT. Determining similar limits to
 371 yield a predominance of nightside reconnection is more difficult. As noted above, high
 372 magnitude *SML* tends to require ongoing dayside driving, such that below values of \sim
 373 -200 nT *dMLT* tends to reduce. Nevertheless, some *SML* enhancement is required,
 374 or else *dMLT* may be less than 12 h even for positive IMF B_Z . As negative B_Z will al-

ways produce a component of dayside reconnection driven flow, we thus opted for positive B_Z and modest negative SML as a filter for nightside reconnection dominated flow.

Returning then, to the distributions of foci locations, we now discuss the data subsets for dominant dayside or nightside reconnection driven flows shown in Figure 2b-c. The latitudes of the foci seem to vary as predicted by the ECPC model, being higher when we might expect dayside reconnection to dominate (Figure 2b), and being lower when we might expect nightside reconnection to dominate (Figure 2c). The reason for our expectations is based on the assumption that nightside reconnection only becomes significant once the polar cap has expanded, due to an accumulation of open flux. Prior to such an accumulation, when the polar cap will be smaller, we thus expect dayside reconnection to dominate. The expansion and contraction of the polar cap in association with dayside and nightside reconnection is not a new finding, having been demonstrated with respect to the substorm cycle in auroral (e.g. Milan et al., 2009), field-aligned current (e.g. Coxon et al., 2014) and convection data (e.g. Grocott et al., 2009), tested using radar observations (e.g. Walach et al., 2017; Sotirelis et al., 2017), and recently studied in detail over an extended interval by Milan et al. (2021). Here we simply note that the convection cell foci latitudes seem to obey the same basic behaviour.

The main focus of our analysis has concerned the local times of the convection cell foci. According to the ECPC model, as discussed theoretically by Cowley and Lockwood (1992), and later modelled numerically (e.g. Freeman & Morley, 2004; Lockwood & Morley, 2004; Lockwood et al., 2006; Milan et al., 2013; Walach et al., 2017), dayside and nightside reconnection each drive an independent component of the ionospheric convection pattern. The foci of the convection cells are expected to lie at the ends of the ionospheric projection of the reconnection line, hence, for dayside reconnection driven flow the foci are expected to be located on the dayside and for nightside reconnection driven flow the foci are expected to be located on the nightside. We see some evidence for this in Figure 2b-c, with the peaks of the foci distributions being located (just) on the dayside in Figure 2b and further round to the nightside in Figure 2c. The effect is perhaps clearer in the distributions of $dMLT$ shown in Figure 4b, in which the distributions of subsets filtered for dominant dayside and nightside reconnection are clearly separated. Nonetheless, significant overlap of the distributions is also apparent, suggesting that either our choice of filter values is imperfect (quite likely) or that the $dMLT$ parameter is itself inadequate to fully capture the convection cell behaviour (also quite likely).

To investigate the latter, we further probed the local time distributions of the dawn and dusk convection cell foci in Figure 5. An offset to the distribution corresponding to a clockwise rotation was noted, that might be partly responsible for the differing behaviour of the dawn and dusk foci mentioned above. Furthermore, we should note that this also implies a discrepancy between any discussion of dayside or nightside foci, and the use of $dMLT < 0$ or $dMLT > 0$, since any rotation could move both cell foci between the dayside and nightside without any change to $dMLT$. One factor known to introduce a clockwise rotation to the convection pattern is IMF $B_Y > 0$ (e.g. Grocott et al., 2012). Figure 2f revealed a B_Y -dependence of the foci locations, but an opposite one at dawn and dusk, thus corresponding to a rotation rather than a shift of both foci towards the dayside or nightside. We checked whether the inherent clockwise rotation might be due to any bias in the prevalence of IMF B_Y in the intervals studied. We found that only 47% of the intervals had $B_Y > 0$ and 53% had $B_Y < 0$, suggesting that the observed average clockwise rotation not due to IMF B_Y . This is also consistent with the findings of Grocott et al. (2012) who found a similar B_Y -independent clockwise rotation. To check for any significance to the potential bias in the dawn and dusk foci locations we can turn to Figure 5b-c. Here we showed the distributions of the foci local times for the dayside and nightside reconnection driven subsets separately. Whilst there is some spread in each case, the two subsets barely overlap, suggesting that they represent distinct populations.

We finally return briefly to the transpolar voltage data presented in Figure 4a. It was shown above that V_{PC} peaks occur at $dMLT$ values of ~ 11 h and ~ 13 h. That there is a local minimum at 12 h is consistent with a steady state of balanced dayside and nightside reconnection being less common than a dominance of either dayside or nightside driving. That the peak V_{PC} values decrease away from $dMLT = 12$ h, where we expect more dominant day or nightside driving is also consistent with the ECPC model. According to Lockwood (1991) V_{PC} is related to the dayside and nightside reconnection rates, V_D and V_N , by

$$V_{PC} = \frac{V_D + V_N}{2} \quad (1)$$

such that, for the case where either V_D or V_N is zero, V_{PC} is equal to half of the rate of the active reconnection line. If we assume that the most extreme $dMLT$ values correspond to the most imbalanced reconnection, then we might expect V_{PC} to be approximately half its peak value at these extremes.

5 Conclusions

In this paper we have presented an analysis of the locations of the foci of the twin-vortex ionospheric convection cells using a 20 year archive of SuperDARN radar observations. We filtered the data to include only intervals of particularly high backscatter echoes ($n > 250$) and also only intervals where the negative cell focus was constrained to 12–24 MLT and the positive cell focus to 0–12 MLT, consistent with Dungey cycle twin-vortex flow. We can conclude that the SuperDARN convection maps capture a wide spread of foci locations and that the locations are sensitive to both IMF B_Z and the SML index. This suggests that the cell foci locations are responding to differing rates of dayside and nightside reconnection. We further filtered the data by suitable ranges of B_Z and SML to isolate one population that is dominated by dayside reconnection and another dominated by nightside reconnection. Analysis of these data provides evidence that the response is consistent with the predictions of the expanding-contracting polar cap model. First, the foci tend to cluster at higher latitudes when dayside reconnection dominates, and lower latitudes when nightside reconnection dominates. Second, the hour angle between the dawn and dusk foci, $dMLT$, is reduced (foci closer to noon) when dayside reconnection dominates, and increases (foci closer to midnight) when nightside reconnection dominates.

We draw a number of further conclusions. The relationship between the foci local times and the SML index is not straightforward. We find that, at a fixed level of SML , $dMLT$ decreases with increasingly negative IMF B_Z . We also find that, at a fixed level of IMF B_Z , $dMLT$ increases with increasingly negative SML , but only up to modest values of SML (to ~ -200 nT). As SML becomes further enhanced $dMLT$ decreases again. We attribute this to an inherent dependence of SML on IMF B_Z in that, for SML to reach strongly negative values, B_Z must also be negative. In other words, episodes of intense nightside reconnection (and associated open flux closure) only occur if there has been, and is likely ongoing, persistent dayside reconnection (and open flux production). Only for relatively modest levels of dayside reconnection can nightside reconnection dominate. This interdependency complicates efforts to isolate the nightside component of the flow. The dayside component is easier to isolate, as it takes some time for nightside reconnection to become enhanced following the onset of dayside reconnection.

Open Research

SuperDARN data was accessed via the British Antarctic Survey data archive (<https://www.bas.ac.uk/projects>) Other data mirrors are hosted by the Virginia Tech SuperDARN group (<http://vt.superdarn.org/>) and the University of Saskatchewan (<https://superdarn.ca/data-download>). The radar data fitting and spherical harmonic analysis were performed using the FITACF2.5 library

475 and version 4.2 of the Radar Software Toolkit (RST) (SuperDARN Data Analysis Work-
476 ing Group et al., 2018). The Map Potential data processing is described fully in (Walach
477 et al., 2022) and we use the equivalent of their ‘D4’ dataset. All solar wind data were
478 downloaded from NASA’s SPDF Coordinated Data Analysis Web (<https://cdaweb.gsfc.nasa.gov/index.html/>)
479 The SML auroral electrojet index used in this paper was provided by the SuperMAG
480 collaboration (<https://supermag.jhuapl.edu>) (Newell & Gjerloev, 2011).

481 Acknowledgments

482 The authors gratefully acknowledge the use of SuperDARN data. SuperDARN is a col-
483 lection of radars funded by national scientific funding agencies of Australia, Canada, China,
484 France, Italy, Japan, Norway, South Africa, United Kingdom, and United States of Amer-
485 ica, and we thank the international PI team for providing the data. We also gratefully
486 acknowledge the SuperMAG collaborators (<https://supermag.jhuapl.edu/info/?page=acknowledgement>)
487 for the SML data, and the ACE MAG and SWEPAM instrument teams, and the ACE
488 Science Center, for providing the ACE data. We gratefully acknowledge the use of The
489 High End Computing facility at Lancaster University which has facilitated the neces-
490 sary data processing for this study. A. Grocott and M.-T. Walach were supported by Nat-
491 ural Environment Research Council (NERC), UK, grant nos. NE/T000937/1 and NE/V00283X/1.
492 S. Milan was supported by the Science and Technology Facilities Council (STFC), UK,
493 grant no. ST/W00089X/1. For the purpose of open access, the author(s) has applied a
494 Creative Commons Attribution (CC BY) licence to any Author Accepted Manuscript
495 version arising.

References

- 496
497 Borovsky, J. E., Hesse, M., Birn, J., & Kuznetsova, M. M. (2008). What de-
498 termines the reconnection rate at the dayside magnetosphere? *Journal of*
499 *Geophysical Research: Space Physics*, *113*(A7). Retrieved from [https://](https://agupubs.onlinelibrary.wiley.com/doi/abs/10.1029/2007JA012645)
500 agupubs.onlinelibrary.wiley.com/doi/abs/10.1029/2007JA012645 doi:
501 <https://doi.org/10.1029/2007JA012645>
- 502 Boyle, C. B., Reiff, P. H., & Hairston, M. R. (1997, January). Empirical polar cap
503 potentials. *J. Geophys. Res.*, *102*(A1), 111-125.
- 504 Chisham, G., Lester, M., Milan, S. E., Freeman, M. P., Bristow, W. A., Gro-
505 cott, A., ... Walker, A. D. M. (2007, January). A decade of the Super
506 Dual Auroral Radar Network (SuperDARN): scientific achievements, new
507 techniques and future directions. *Surveys in Geophysics*, *28*, 33-109. doi:
508 [10.1007/s10712-007-9017-8](https://doi.org/10.1007/s10712-007-9017-8)
- 509 Cowley, S. W. H., & Lockwood, M. (1992, February). Excitation and decay of solar
510 wind-driven flows in the magnetosphere-ionosphere system. *Ann. Geophysicae*,
511 *10*, 103-115.
- 512 Coxon, J. C., Milan, S. E., Clausen, L. B. N., Anderson, B. J., & Korth, H.
513 (2014). A superposed epoch analysis of the regions 1 and 2 birkeland cur-
514 rents observed by ampere during substorms. *Journal of Geophysical Re-*
515 *search: Space Physics*, *119*(12), 9834-9846. Retrieved from [https://](https://agupubs.onlinelibrary.wiley.com/doi/abs/10.1002/2014JA020500)
516 agupubs.onlinelibrary.wiley.com/doi/abs/10.1002/2014JA020500 doi:
517 <https://doi.org/10.1002/2014JA020500>
- 518 Davis, T. N., & Sugiura, M. (1966). Auroral electrojet activity index *ae* and its uni-
519 versal time variations. *J. Geophys. Res.*, *71*(785).
- 520 Etemadi, A., Cowley, S. W. H., Lockwood, M., Bromage, B. J. I., Willis, D. M.,
521 & Luhr, H. (1988, May). The dependence of high-latitude dayside iono-
522 spheric flows on the north south component of the IMF - a high time resolu-
523 tion correlation-analysis using EISCAT POLAR and AMPTE UKS and IRM
524 data. *Planet. Space Sci.*, *36*(5), 471-498.
- 525 Feldstein, Y. I., & Starkov, G. V. (1967). Dynamics of auroral belt and polar geo-
526 magnetic disturbances. *Planet. Space Sci.*, *18*, 401-454.
- 527 Fogg, A. R., Lester, M., Yeoman, T. K., Burrell, A. G., Imber, S. M., Milan, S. E.,
528 ... Anderson, B. J. (2020, MAY). An improved estimation of superdarn
529 heppner-maynard boundaries using ampere data. *JOURNAL OF GEOPHYSI-*
530 *CAL RESEARCH-SPACE PHYSICS*, *125*(5). doi: [10.1029/2019JA027218](https://doi.org/10.1029/2019JA027218)
- 531 Freeman, M. P., & Morley, S. K. (2004). A minimal substorm model that explains
532 the observed statistical distribution of times between substorms. *Geophysical*
533 *Research Letters*, *31*(12). Retrieved from [https://agupubs.onlinelibrary](https://agupubs.onlinelibrary.wiley.com/doi/abs/10.1029/2004GL019989)
534 [.wiley.com/doi/abs/10.1029/2004GL019989](https://agupubs.onlinelibrary.wiley.com/doi/abs/10.1029/2004GL019989) doi: [https://doi.org/10.1029/](https://doi.org/10.1029/2004GL019989)
535 [2004GL019989](https://doi.org/10.1029/2004GL019989)
- 536 Gjerloev, J. W. (2012). The supermag data processing technique. *Journal of Geo-*
537 *physical Research: Space Physics*, *117*(A9). Retrieved from [https://agupubs](https://agupubs.onlinelibrary.wiley.com/doi/abs/10.1029/2012JA017683)
538 [.onlinelibrary.wiley.com/doi/abs/10.1029/2012JA017683](https://agupubs.onlinelibrary.wiley.com/doi/abs/10.1029/2012JA017683) doi: [https://](https://doi.org/10.1029/2012JA017683)
539 doi.org/10.1029/2012JA017683
- 540 Gordeev, E. I., Sergeev, V. A., Pulkkinen, T. I., & Palmroth, M. (2011). Contribu-
541 tion of magnetotail reconnection to the cross-polar cap electric potential
542 drop. *Journal of Geophysical Research: Space Physics*, *116*(A8). Retrieved
543 from [https://agupubs.onlinelibrary.wiley.com/doi/abs/10.1029/](https://agupubs.onlinelibrary.wiley.com/doi/abs/10.1029/2011JA016609)
544 [2011JA016609](https://agupubs.onlinelibrary.wiley.com/doi/abs/10.1029/2011JA016609) doi: <https://doi.org/10.1029/2011JA016609>
- 545 Greenwald, R. A., Baker, K. B., Dudeney, J. R., Pinnock, M., Jones, T. B., Thomas,
546 E. C., ... Yamagishi, H. (1995, February). Darn/SuperDarn: A global view
547 of the dynamics of high-latitude convection. *Space Sci. Rev.*, *71*, 761-796. doi:
548 [10.1007/BF00751350](https://doi.org/10.1007/BF00751350)
- 549 Greenwald, R. A., Ruohoniemi, J. M., Baker, K. B., Bristow, W. A., Sofko,
550 G. J., Villain, J.-P., ... Slavin, J. A. (1999). Convective response to a

- 551 transient increase in dayside reconnection. *Journal of Geophysical Re-*
 552 *search: Space Physics*, 104(A5), 10007-10015. Retrieved from [https://](https://agupubs.onlinelibrary.wiley.com/doi/abs/10.1029/98JA02723)
 553 agupubs.onlinelibrary.wiley.com/doi/abs/10.1029/98JA02723 doi:
 554 <https://doi.org/10.1029/98JA02723>
- 555 Greenwald, R. A., Ruohoniemi, J. M., Bristow, W. A., Sofko, G. J., Villain, J.-P.,
 556 Huuskonen, A., ... Frank, L. A. (1996, October). Mesoscale dayside convec-
 557 tion vortices and their relation to substorm phase. *J. Geophys. Res.*, 101(A10),
 558 21697-21713.
- 559 Grocott, A., Cowley, S. W. H., & Sigwarth, J. B. (2003, February). Ionospheric flow
 560 during extended intervals of northward but B_Y -dominated IMF. *Ann. Geo-*
 561 *physicae*, 21, 509-538.
- 562 Grocott, A., Cowley, S. W. H., Sigwarth, J. B., Watermann, J. F., & Yeoman, T. K.
 563 (2002, October). Excitation of twin-vortex flow in the nightside high-latitude
 564 ionosphere during an isolated substorm. *Ann. Geophysicae*, 20, 1577-1601.
- 565 Grocott, A., Milan, S. E., Imber, S. M., Lester, M., & Yeoman, T. K. (2012). A
 566 quantitative deconstruction of the morphology of high-latitude ionospheric
 567 convection. *J. Geophys. Res.*, 117(A5). Retrieved from [http://dx.doi.org/](http://dx.doi.org/10.1029/2012JA017580)
 568 [10.1029/2012JA017580](http://dx.doi.org/10.1029/2012JA017580) doi: 10.1029/2012JA017580
- 569 Grocott, A., Wild, J. A., Milan, S. E., & Yeoman, T. K. (2009). Superposed epoch
 570 analysis of the ionospheric convection evolution during substorms: onset lati-
 571 tude dependence. *Ann. Geophysicae*, 27(2), 591-600.
- 572 Heppner, J. P., & Maynard, N. C. (1987, May). Empirical high-latitude electric-field
 573 models. *J. Geophys. Res.*, 92(A5), 4467-4489.
- 574 Imber, S. M., Milan, S. E., & Lester, M. (2013). The Heppner-Maynard Bound-
 575 ary measured by SuperDARN as a proxy for the latitude of the auroral oval.
 576 *J. Geophys. Res.*, 118(2), 685-697. doi: 10.1029/2012JA018222
- 577 Iyemori, T. (1990). Storm-time magnetospheric currents inferred from mid-latitude
 578 geomagnetic field variations. *Journal of geomagnetism and geoelectricity*,
 579 42(11), 1249-1265. doi: 10.5636/jgg.42.1249
- 580 Lockwood, M. (1991). On flow reversal boundaries and transpolar voltage in average
 581 models of high-latitude convection. *Planetary and Space Science*, 39(3), 397-
 582 409.
- 583 Lockwood, M., Lanchester, B. S., Morley, S. K., Throp, K., Milan, S. E., Lester,
 584 M., & Frey, H. U. (2006). Modeling the observed proton aurora and iono-
 585 spheric convection responses to changes in the imf clock angle: 2. persistence
 586 of ionospheric convection. *Journal of Geophysical Research: Space Physics*,
 587 111(A2). Retrieved from [https://agupubs.onlinelibrary.wiley.com/doi/](https://agupubs.onlinelibrary.wiley.com/doi/abs/10.1029/2003JA010307)
 588 [abs/10.1029/2003JA010307](https://agupubs.onlinelibrary.wiley.com/doi/abs/10.1029/2003JA010307) doi: <https://doi.org/10.1029/2003JA010307>
- 589 Lockwood, M., & McWilliams, K. A. (2021, SEP). A survey of 25 years' transpolar
 590 voltage data from the superdarn radar network and the expanding-contracting
 591 polar cap model. *JOURNAL OF GEOPHYSICAL RESEARCH-SPACE*
 592 *PHYSICS*, 126(9). doi: 10.1029/2021JA029554
- 593 Lockwood, M., & Morley, S. K. (2004). A numerical model of the ionospheric sig-
 594 natures of time-varying magnetic reconnection: I. ionospheric convection. *Ann.*
 595 *Geophys.*, 22(1), 73-91.
- 596 MacDougall, J. W., & Jayachandran, P. T. (2001). Polar cap convection rela-
 597 tionships with solar wind. *Radio Science*, 36(6), 1869-1880. Retrieved
 598 from [https://agupubs.onlinelibrary.wiley.com/doi/abs/10.1029/](https://agupubs.onlinelibrary.wiley.com/doi/abs/10.1029/2001RS001007)
 599 [2001RS001007](https://agupubs.onlinelibrary.wiley.com/doi/abs/10.1029/2001RS001007) doi: <https://doi.org/10.1029/2001RS001007>
- 600 Milan, S. E., Carter, J. A., Sangha, H., Bower, G. E., & Anderson, B. J.
 601 (2021). Magnetospheric flux throughput in the dungey cycle: Identifi-
 602 cation of convection state during 2010. *Journal of Geophysical Re-*
 603 *search: Space Physics*, 126(2), e2020JA028437. Retrieved from [https://](https://agupubs.onlinelibrary.wiley.com/doi/abs/10.1029/2020JA028437)
 604 agupubs.onlinelibrary.wiley.com/doi/abs/10.1029/2020JA028437
 605 (e2020JA028437 2020JA028437) doi: <https://doi.org/10.1029/2020JA028437>

- 606 Milan, S. E., Gosling, J. S., & Hubert, B. (2012, MAR 28). Relationship between
 607 interplanetary parameters and the magnetopause reconnection rate quantified
 608 from observations of the expanding polar cap [Article]. *J. Geophys. Res.*, *117*.
 609 doi: {10.1029/2011JA017082}
- 610 Milan, S. E., Grocott, A., de Larquier, S., Lester, M., Yeoman, T. K., Freeman,
 611 M. P., & Chisham, G. (2013). Travelling ionospheric disturbances in the Wed-
 612 dell Sea Anomaly associated with geomagnetic activity. *J. Geophys. Res.*, *118*.
 613 doi: 10.1002/jgra.50566,
- 614 Milan, S. E., Grocott, A., Forsyth, C., Imber, S. M., Boakes, P. D., & Hubert, B.
 615 (2008, August). Looking through the oval window. *Astronomy and Geophysics*,
 616 *49*(4), 4.16-4.18. doi: 10.1111/j.1468-4004.2008.49416.x
- 617 Milan, S. E., Grocott, A., Forsyth, C., Imber, S. M., Boakes, P. D., & Hubert, B.
 618 (2009). A superposed epoch analysis of auroral evolution during substorm
 619 growth, onset and recovery: open magnetic flux control of substorm intensity.
 620 *Ann. Geophysicae*, *27*(2), 659-668.
- 621 Nakai, H., & Kamide, Y. (2003). Substorm-associated large-scale magnetic
 622 field changes in the magnetotail: a prerequisite for "magnetotail defla-
 623 tion" events. *Annales Geophysicae*, *21*(4), 869–879. Retrieved from
 624 <https://angeo.copernicus.org/articles/21/869/2003/> doi: 10.5194/
 625 angeo-21-869-2003
- 626 Newell, P. T., & Gjerloev, J. W. (2011). Evaluation of supermag auroral elec-
 627 trojet indices as indicators of substorms and auroral power. *Journal of*
 628 *Geophysical Research: Space Physics*, *116*(A12). Retrieved from [https://](https://agupubs.onlinelibrary.wiley.com/doi/abs/10.1029/2011JA016779)
 629 agupubs.onlinelibrary.wiley.com/doi/abs/10.1029/2011JA016779 doi:
 630 <https://doi.org/10.1029/2011JA016779>
- 631 Press, W. H., Teukelosky, S. A., Vetterling, W. T., & Flannery, B. P. (2007). *Nu-*
 632 *merical recipes: The art of scientific computing* (3rd ed.). Cambridge, U.K.:
 633 Cambridge Univ. Press.
- 634 Ruohoniemi, J. M., & Baker, K. B. (1998, September). Large-scale imaging of
 635 high-latitude convection with Super Dual Auroral Radar Network HF radar
 636 observations. *J. Geophys. Res.*, *103*, 20797-20811. doi: 10.1029/98JA01288
- 637 Ruohoniemi, J. M., & Greenwald, R. A. (2005, September). Dependencies of high-
 638 latitude plasma convection: Consideration of interplanetary magnetic field,
 639 seasonal, and universal time factors in statistical patterns. *J. Geophys. Res.*,
 640 *110*(A9). doi: 10.1029/2004JA010815
- 641 Shepherd, S., & Ruohoniemi, J. (2000, October). Electrostatic potential patterns
 642 in the high-latitude ionosphere constrained by SuperDARN measurements.
 643 *J. Geophys. Res.*, *105*(A10), 23005-23014.
- 644 Smith, C. W., L'Heureux, J., Ness, N. F., Acuña, M. H., Burlaga, L. F., & Scheifele,
 645 J. (1998, July). The ACE magnetic fields experiment. *Space Sci. Rev.*, *86*,
 646 613-632. doi: 10.1023/A:1005092216668
- 647 Sotirelis, T., Keller, M. R., Liou, K., Smith, D., Barnes, R. J., Talaat, E., & Baker,
 648 J. B. H. (2017). Testing the expanding-contracting polar cap paradigm. *Jour-*
 649 *nal of Geophysical Research: Space Physics*, *122*(7), 7077-7086. Retrieved
 650 from [https://agupubs.onlinelibrary.wiley.com/doi/abs/10.1002/](https://agupubs.onlinelibrary.wiley.com/doi/abs/10.1002/2017JA024238)
 651 [2017JA024238](https://doi.org/10.1002/2017JA024238) doi: <https://doi.org/10.1002/2017JA024238>
- 652 Stone, E. C., Frandsen, A. M., Mewaldt, R. A., Christian, E. R., Margolies, D.,
 653 Ormes, J. F., & Snow, F. (1998, July). The Advanced Composition Explorer.
 654 *Space Sci. Rev.*, *86*, 1-22. doi: 10.1023/A:1005082526237
- 655 SuperDARN Data Analysis Working Group, Thomas, E. G., Ponomarenko, P. V.,
 656 Billett, D. D., Bland, E. C., Burrell, A. G., & Walach, M.-T. (2018). *Su-*
 657 *perdarn radar software toolkit (rst) (version 4.2) [software]*. doi: 10.5281/
 658 zenodo.1403226
- 659 Thomas, E. G., & Shepherd, S. G. (2018, April). Statistical Patterns of Ionospheric
 660 Convection Derived From Mid-latitude, High-Latitude, and Polar SuperDARN

- 661 HF Radar Observations. *J. Geophys. Res-Space Phys.*, 123(4), 3196–3216. doi:
662 10.1002/2018JA025280
- 663 Walach, M.-T., & Grocott, A. (2019). Superdarn observations during geomagnetic
664 storms, geomagnetically active times, and enhanced solar wind driving. *Jour-*
665 *nal of Geophysical Research: Space Physics*, 124(7), 5828–5847. Retrieved
666 from [https://agupubs.onlinelibrary.wiley.com/doi/abs/10.1029/
667 2019JA026816](https://agupubs.onlinelibrary.wiley.com/doi/abs/10.1029/2019JA026816) doi: <https://doi.org/10.1029/2019JA026816>
- 668 Walach, M.-T., Grocott, A., Staples, F., & Thomas, E. G. (2022). Super dual au-
669 roral radar network expansion and its influence on the derived ionospheric
670 convection pattern. *Journal of Geophysical Research: Space Physics*, 127(2),
671 e2021JA029559. Retrieved from [https://agupubs.onlinelibrary.wiley
672 .com/doi/abs/10.1029/2021JA029559](https://agupubs.onlinelibrary.wiley.com/doi/abs/10.1029/2021JA029559) (e2021JA029559 2021JA029559) doi:
673 <https://doi.org/10.1029/2021JA029559>
- 674 Walach, M.-T., Milan, S. E., Yeoman, T. K., Hubert, B. A., & Hairston, M. R.
675 (2017). Testing nowcasts of the ionospheric convection from the expanding and
676 contracting polar cap model. *Space Weather*, 15(4), 623–636. Retrieved
677 from [https://agupubs.onlinelibrary.wiley.com/doi/abs/10.1002/
678 2017SW001615](https://agupubs.onlinelibrary.wiley.com/doi/abs/10.1002/2017SW001615) doi: <https://doi.org/10.1002/2017SW001615>
- 679 Weimer, D. R. (2005, May). Improved ionospheric electrodynamic models and
680 application to calculating joule heating rates. *J. Geophys. Res-Space Phys.*,
681 110(A5). doi: 10.1029/2004JA010884